UNMANNED VTOL PROPULSION RESEARCH – SCALABILITY OF QUADCOPTER ROTOR-MOTOR CONFIGURATIONS OUTSIDE THE sUAS REGIME

Kendy Edmonds,[1] D. Blake Stringer,[2]

Consumer-based sUAS or "drone" products with a useful load under 55-lbs use variable-speed rotor-motor configurations to provide lift and thrust. The feasibility of these variable-speed configurations is unknown in the commercial/military UAS design space as the quadcopter-type platform grows between 100 and 1,000 lbf useful load. As the size of the rotor-motor configurations increase, so does the inertia. It is unclear what the effects of the increased inertia are on the transient response of the variable-speed configurations. This paper presents the results of an experimental study investigating the transient response of different sized rotor-motor configurations. A series of experiments on different rotor-motor combinations was conducted. The transient response as well as the parameters of over 35 variables were recorded. The data is presented and discussed, clearly showing a relationship between the transient settling time of a sUAS and its rotor inertia.

INTRODUCTION

The rapid proliferation and success of quadcopter and other vertical-takeoff-and-landing (VTOL) configurations in the consumer market culminated in the release of Federal Aviation Administration Part 107 for regulatory guidance on the legal operation of small Unmanned Aircraft Systems (sUAS) [1]. At the same time, however, the disadvantages of these quadcopter configurations became apparent as well, specifically the problems of power and endurance [2]–[4].

Nevertheless, sUAS VTOL configurations have proven their feasibility as a platform for several applications to include logistics and payload delivery [2], [3]. The potential exists to design and build platforms to carry greater payloads with higher range and endurance capabilities, especially in challenging terrain and operating conditions. This potential also exists in military applications.

With DOD projected expenditures of $4.5B in new unmanned aircraft research and procurement initiatives toward capability improvements [5], along with the commercialized drone activities of corporations such as Amazon and UPS [2], [6], it is critical to determine the scalability of current sUAS propulsion methods to support these larger platforms.

Modern sUAS are propelled by electric, DC, fixed-pitch, variable-speed motors, while traditional rotorcraft are powered using variable-pitch, constant-speed rotor systems. One consideration in scaling is the transient behavior of the motor-rotor system. As the platform increases in size, so too does the rotors and electric motors, leading to an increase in the rotational

[1] Research Assistant, College of Aeronautics & Engineering, Kent State University, Kent, Ohio 44242.
[2] Assistant Professor, College of Aeronautics & Engineering, Kent State University, Kent, Ohio 44242.

inertia of the propulsion system. The increased inertia intuitively means that the larger systems do not respond as quickly as smaller rotors [7].

The purpose of this paper is to present the results of a study objective of this research effort has been to experimentally measure and quantify the transient response of variable-speed rotor-motor configurations through (1) construction of a table-top experimental rotor-motor static test stand, (2) demonstration of data extraction capabilities, (3) performance characterization of varying-size rotor and disk diameters, and (4) determination of static test bench scalability.

BACKGROUND

Power Scaling Requirements

For purposes of this research, it has been assumed that the unmanned VTOL platform scales in size to operate within the Group III UAS regime. The Group III UAS regime is defined at a maximum gross takeoff weight of 1,320 lbf, a maximum operating altitude of 18,000 ft MSL, with no airspeed restrictions. This roughly corresponds to an aircraft with maximum payload of 400 lbf and a range-radius from 50 - 1,000 nm [8]. However, this is not the upper limit of the applications of this study. The platform could easily cross the threshold into the Group IV UAS category: greater than 1,320 lbf, and below 18,000 ft MSL. Additionally, the feasibility of large variable-speed rotor-motors could also be applied to urban air transport development aircraft, such as those advocated by Uber [9].

Quadcopter-type power requirements increase drastically as size increases, as illustrated in Figure 1. The figure displays two contour plots for the variation of hover-power requirements of a quadcopter as a function of weight and disk loading. The triangular data point represents the location of a familiar drone in this regime, the Phantom 3 Professional, offered by DJI. The inverted triangle represents the R-22 helicopter, which has a similar payload capacity to the nominal UAS platform and is represented by the circle. This nominal aircraft assumes four 36-in diameter rotors and 1,000-lbf gross weight. The comparison of these three platforms is presented in Table 1.

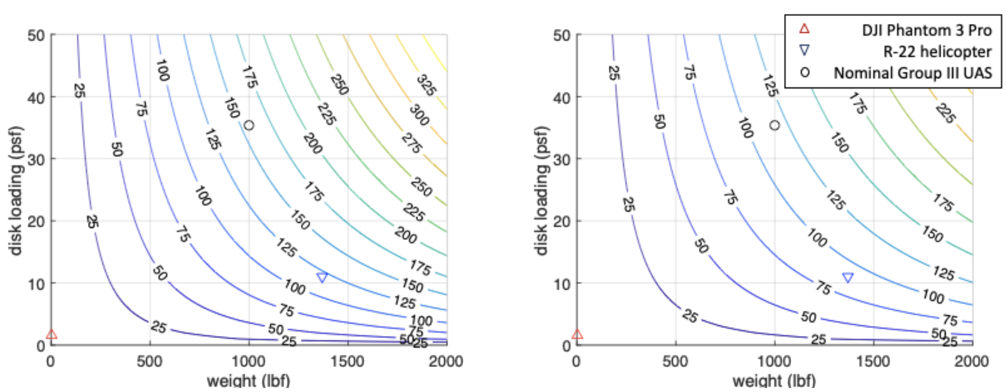

Figure 1: Hover-power requirements versus weight and disk-loading in hp (left) and kW(right)

Table 1: Platform hover power comparison

	DJI Phantom III	**R-22 Helicopter**	**Group III UAS**
Disk loading (T/A)	1.6 psf	11.0 psf	35.4 psf
Gross weight (W)	2.82 lbf	1,370 lbf	1,000 lbf
Hover power (P_h)	0.094 hp (0.070 kW)	120 hp (89.5 kW)	157 hp (117 kW)
Maneuver power (P_m)	0.266 hp (0.199 kW)	339 hp (253 kW)	444 hp (331 kW)

The hover-power requirements do not include any transient requirements for maneuvering the aircraft, especially abrupt maneuvering. Conventional small UAS design calculations generally assume doubling the thrust to ensure adequate power [10]. This technique essentially models a 2G maneuver. Using this rule-of-thumb for the nominal platform results in a transient power requirement of 444 hp (331 kW). This is a 283% increase over its hover-power requirement in Table 1. It is evident from the data presented in Figure 1 and Table 1 that the hover and maneuver power requirements greatly increase with size.

There are some important items to note in this analysis: (1) As the size of the aircraft grows, increasing rotor diameter assists in maintaining manageable power requirements. (2) As the size of the rotors increases, so do the power requirements for spinning the rotors to overcome inertia and blade profile drag. These increased power requirements are in addition to the hover-power requirements of Table 1.

Consequently, there are three questions for scaling quadcopter-type applications using variable-speed motors.

1. At what size rotor-motor system does the inertia noticeably affect the transient time between different motor speeds?
2. Based upon the results from No. 1, what is the maximum rotor diameter that can effectively use variable speed motors?
3. How do these transient conditions affect and determine maneuverability?

The State-of-the-Art in 2018

A review of the literature has not yielded much information on current or previous studies on the scalability of variable-speed rotors, indicating this is a relatively untouched focus area of rotary-wing propulsion. Much of the current research discussing rotor inertia in quadcopter applications use the inertia as a parameter for determining other parameters [11]–[16]. Some authors do provide data on the impacts of rotor inertia and its importance to maneuvering characteristics [17]–[19]. However, these discussions still fall within the very low end of the sUAS regime. By and large, many discussions of transients in the literature focus on the stability and control of the sUAS during transient periods [11]–[16], [20]–[26].

Some transient studies in the literature have focused on fault detection in motors and shafts [27], [28]. The limited nature of material directly applicable in this area may be due to the current focus of quadcopter dynamics in the sUAS regime, where rotor transient impacts are somewhat minimal, except for racing or conditions requiring extreme agility [7]. This research project grew out of an unfunded benchtop construction stand for a student research project [29]. As presented in [29], the focus on rotor inertia "seems to present a gap" in the current state-of-the-art.

METHODOLOGY

Description of Experimental Test Stand

The commercial off-the-shelf (COTS) test stand that was used to capture and record motor parameters was the Series 1780 Thrust Stand and Dynamometer manufactured by RC Benchmark. The static thrust stand is capable of capturing the following: time, electronic-speed-controller pulse-width-modulation (ESC PWM), motor optical speed (RPM), thrust, torque, electrical power in, mechanical power out, temperature of desired components, transient response time, maximum acceleration values, and system efficiency estimations. The limitations of the stand are outlined in Table 2. The stand is surrounded by a plywood shroud with steel plates around the tip-path-plane of the spinning rotor to provide ballistic protection. The test stand itself is presented in Figure 2.

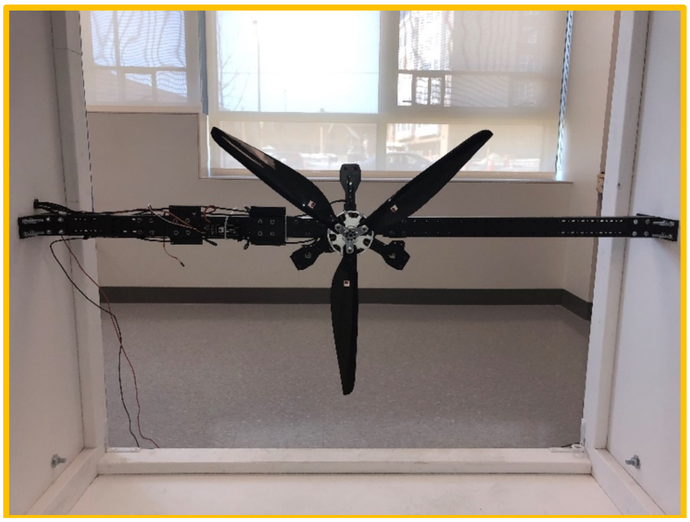

Figure 2: Thrust stand configuration

The thrust stand is controlled via a software package developed by RC Benchmark. The thrust stand is capable of both manual control of the motor and automated testing and data recording. The voltage is regulated by connecting 12.0V batteries in series, with a minimum configuration of one battery and maximum of five. This configuration was adequate for the tests required for this study.

Table 2: Thrust Stand Limitations

Parameter	Limitation	Units
Voltage	0 – 60	Volts
Current	100	Amps
Optical Speed	190,000	RPM
Thrust	55	Pounds
Torque	7.39	Foot-pounds

Rotor-Motor Configurations

Figure 4 shows all the motors used for this study. The following is the naming convention used for each motor from left to right: Turnigy (Turnigy RotoMax 150cc), Mega (KDE Direct 10218XF-105), P80 (T-Motor P80 120kv), KDE (KDE Direct 7215XF-135), and Mini (KDE Direct 4215XF-465). The Mini (far-right) motor in Figure 4 is not the actual motor used for this study. The actual "Mini" motor looks like the other two KDE motors but is the approximate diameter of the motor pictured on the far right. The ESC used with Turnigy, Mega, P80, and KDE configurations was the KDE-UAS125UVC (KDE Direct). The ESC used for experiments ran on Mini was the KDE XF-UAS75HVC (KDE Direct). All manufacturer default settings remained the same for both ESCs.

Figure 3: Motors used in experiments

Three different rotors were used in this study. The largest was a carbon fiber 3-blade propeller with a diameter of 30.5 inches and a pitch of 9.7 inches. The 3-blade propeller is manufactured by KDE Direct. The second rotor used was a carbon fiber 2-blade propeller with a diameter and pitch of 27 and 8.8 inches, respectively. This propeller is manufactured by Falcon. The final rotor was a carbon fiber 2 blade propeller with a diameter and pitch of 15 and 5.5 inches, respectively. The smallest of the 3 propellers is manufactured by T-motors.

The properties of the different rotor-motor configurations used in the study are listed in the appendix.

Experimental Characterization and Validation

A series of initial experiments was conducted to characterize and validate the static thrust stand. Manufacturers of larger electric motors often provide a datasheet outlining various parameters, such as RPM, thrust, and motor efficiency, at a variety of power settings. These were used to compare with data recorded from the static thrust stand to verify proper installation of motors and instrumentation each time a new motor was placed on the stand. An example of this characterization data is presented in in Figure 4.

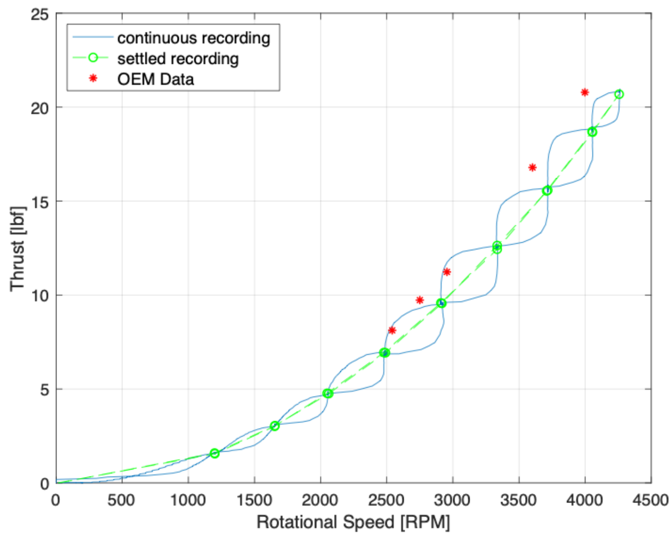

Figure 4: P80 full power Thrust Curve with OEM Data (48 volts)

As mentioned earlier in this paper, the static thrust bench is capable of running a diverse set of automated experiments. The software comes with a variety of pre-configured scripts that can be tailored to specific applications. The main differences between the scripts are the way in which the user controls an experiment. For example, in the pre-configured "Continuous Sweep" script, the user can select the starting and ending throttle setting (indicated by ESC PWM), the time the motor takes to ramp up from the starting throttle to the ending throttle, how long the motor will stay running at the higher throttle setting, and if the script coasts the motor back down to the starting throttle or not.

In contrast, with the built-in "Settling Time" script, the user controls the steps the motor will take in terms of throttle percentage. This script will automatically progress to the next step once the system determines the motor is "settled" and the user cannot control how long it will stay on one throttle percentage input. Variations of the "Settling Time" script were used for the majority of this study, and will be expanded on further.

Some pre-configured, automated scripts, such as the "Settling Time" script, have the option to record all values (returning a CSV file yielding approximately 4 data points per second), or to strictly return one point after the script has determined the system is "settled." In Figure 4, the dashed line is an example of a "settled recording" script, where one point is recorded after the system has settled. The point that is recorded is indicated by the circle. The solid line is an example of a "continuous recording" script, which allows for a visualization of how the rotor(s) ramp up and coast down. For each experiment, both "settled" and "continuous" recording scripts were run for consistency.

Transient Response Experimental Test Matrix

The main experiment used for the purpose of this research was the "Transient Response" experiment, a variation of the pre-configured "Settling Time" script. There were 3 different versions of the Transient Response experiment based upon throttle setting: (1) ramping up from 50% throttle to 75% throttle and coasting back down to 50% throttle, (2) ramping up from 50%

throttle to 90% throttle and coasting back down to 50% throttle, and (3) ramping up from 10% throttle to 90% throttle and coasting back down to 10% throttle.

Each version consisted of 10 pairs of the ramp and coast settings, resulting in a total of 20 usable transient response data points per test. These experiments were chosen to capture both the transient response of drastic changes in motor RPM as well as subtle changes that would be more representative of RPM changes required for basic maneuvering.

The script control goes through a series of checks to ensure that the motor is stabilized before moving on to the next step. It first takes a series of 30 consecutive RPM data points, examines them to see if the series has both increasing and decreasing values, and verifies that the motor stays within +/- 75 RPM. Once this parameter is satisfied, the system records the transient response time and proceeds to the next step. To verify repeatability, each experiment was conducted 3 times. As mentioned earlier, the script also has the option to record all parameter values at a constant rate, or to strictly record all parameter values once, after the system is deemed to be "settled." To ensure all data was captured, and for plotting purposes, each rotor-motor combination was run at each of the settings 3 separate times. This method resulted in a total of 12 experiments for each motor/rotor combination at each power setting. Most motors were run at power settings of 1 to 5 batteries, though some had to be adjusted based upon the individual power limitations.

RESULTS AND DISCUSSION

There are two main topics that will be addressed when discussing the results of this study. The first topic discusses the transient response data. The second topic considers the indirect thermal consequences of running COTS components at high power settings.

Transient Response Data

As mentioned earlier, a variety of experiments were executed on 8 different rotor-motor configurations. Many different, distinct comparisons can be made from these experiments. The plots in Figure 5 illustrates a comparison between the same motor with two different blades installed. The motor used for the experiments illustrated in the left plot is Mega, while the motor used for the second plot is the P80. Both motors are two of the larger motors used in this study. The data points to the right of zero indicate a ramp-up settling time and the data points on the left of zero indicate the coast-down settling time. These plots suggest that inertia of the rotor does play a greater factor in the transient response during coast down in some cases, and in some cases it does not. The points corresponding to a ramp on both plots indicate that blade inertia is not a large factor in the settling time for these configurations.

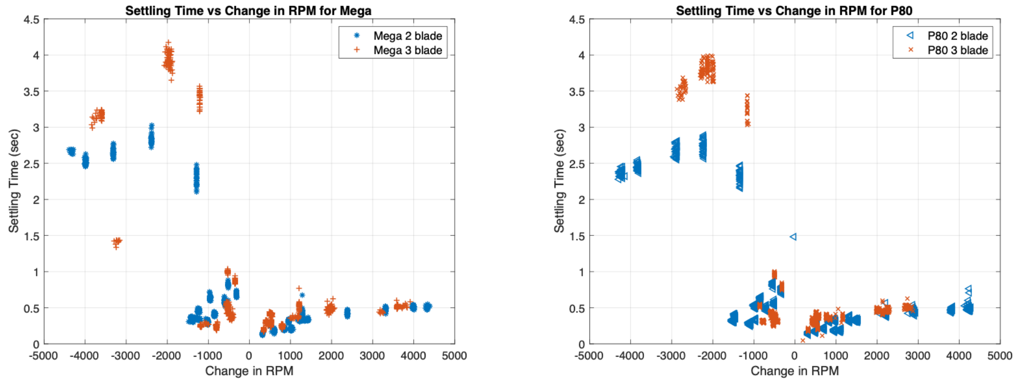

Figure 5: Comparison of settling time for two vs three bladed props

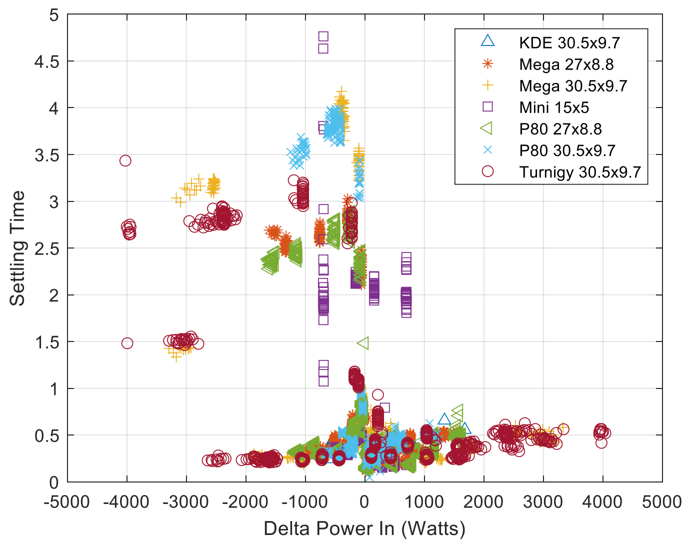

Figure 6: Settling time of all motors plotted against change in power

The results of all the transient response experiments can be seen in Figure 6. Again, the data points to the right of zero indicate a ramp up and the data points on the left of zero indicate a coast down phase. The data points corresponding to the ramp indicate that the transient response of the motor is more significantly impacted when the motor is coasting down and that ramp up time stays fairly even across all rotor-motor combinations. The data points corresponding to the coast down, however, clearly indicate that the motor-rotor configuration matters, as well as the RPM.

There is significantly more variability in the response of each rotor-motor configuration than was expected. For example, in Figure 6, the coast results of the Turnigy 30.5 rotor-motor combination vary widely based upon a change in power. The relationship does not strictly increase or decrease. There are some data points with lower-power changes, yet with high settling times. Similar behavior exists if looking at higher-power changes. These results are strong indicators of the influence of several variables upon the response, not just the rotor inertia.

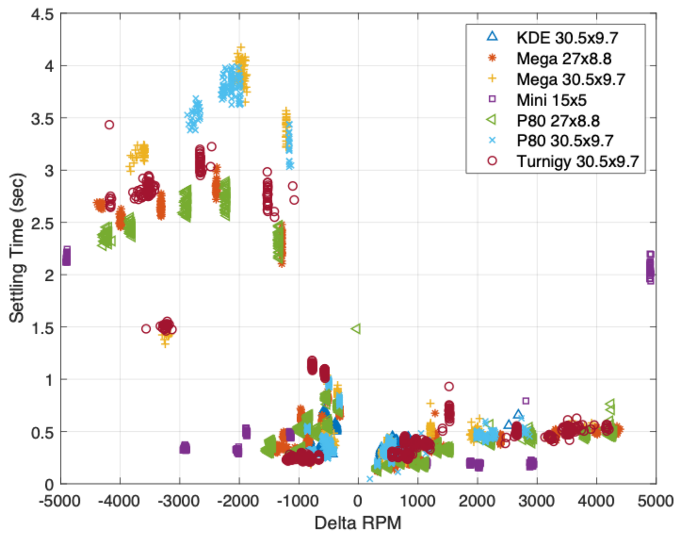

Figure 7: Settling time of all motors plotted against change in RPM

Figure 7 displays the same trends as in Figure 6 for both the coast and the ramp phases. The authors are currently investigating the influence of over 35 input variables on the settling time during the coast phase. This analysis will be conducted using stochastic modeling methods.

For future studies the ability to include more experiments with more of a variation in power changes (and therefore more RPM change variation) would more fully capture trends. Future studies should also include more variety of rotor inertias to capture the significance of the impact rotor inertia has in transient response. It should also be noted that no ESC settings were changed for this study, as the default settings on the ESCs used are suitable for most common applications of UAS. It may be necessary to examine how programming the ESC differently will impact transient response time.

Thermal Considerations

During one experiment, a motor began emitting smoke. Upon further investigation, it was determined that the motor had a manufacturing defect, but this incident brought up an important consideration for running electric motors at high power settings. While the motor is running, the temperature is generally under control. It isn't until the airflow generated by the propellers is taken away that the temperature of the motor will begin to spike up to high, and sometimes unsafe, temperatures.

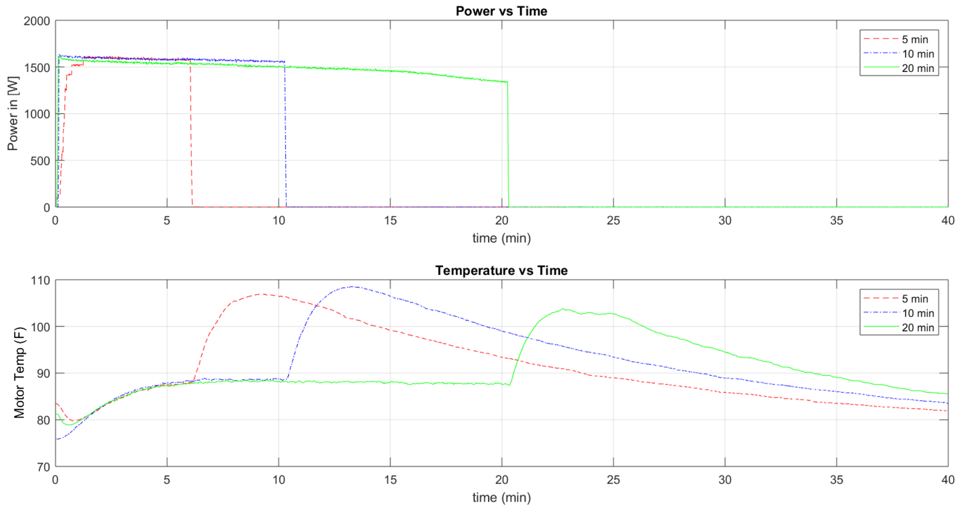

Figure 8: 5, 10, and 20-minute endurance temperature experiments

After the smoke incident, more experiments were conducted to study the effects that different test configurations had on the temperature spike at the end. The two main experiments used to study thermal considerations were endurance and constant power (while varying voltage and current) experiments. An example of the results of an endurance experiment is shown in Figure 9. It is clear from the illustration that the temperature levels off during while the motor is still spinning, and as soon as the power is removed (and the airflow around the motor stops), the temperature spikes up at a steep level.

Running endurance experiments had its limitations due to using batteries as a power supply. Since a constant power source was not used, the larger motors began to draw too much power and drain the batteries during 5, 10, and 15 minute endurance tests. Comparisons for temperature could not be made for larger motor configurations at a constant power since the system was continually draining its power source. Because of this, it was not possible to collect a significant amount of data for endurance experiments. To properly identify trends, it would be necessary to run future experiments with a constant power source.

The other temperature experiment involved running a motor at a constant power value and increasing the voltage to the system (by adding a 12-volt battery in series), thereby decreasing the current supplied to the system. As shown in Figure 9, with the increase in voltage, and therefore decrease in current, the motor still saw an increase of maximum temperature of approximately 1.5 degrees each time there was an increase of approximately 12 volts. These results were consistent with two other motors included in the experimental runs. Though this experiment was conducted on three different rotor-motor combinations, there would still need to be many more experiments with a variety of motors at different power settings to be able to verify this trend.

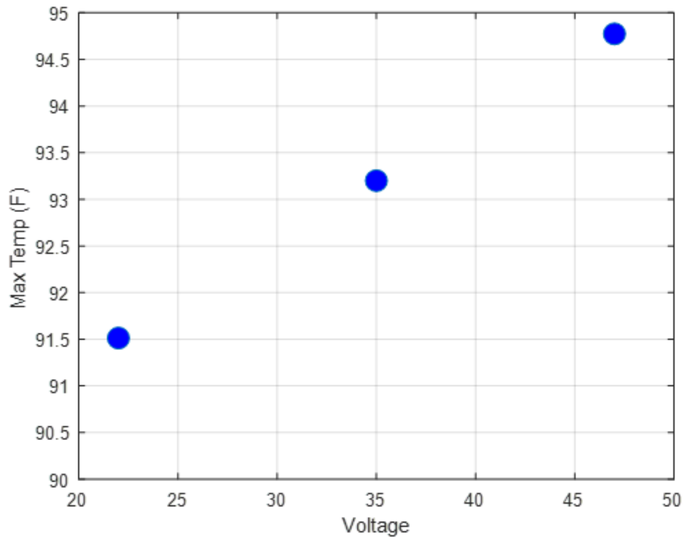

Figure 9: KDE constant power (500 W) temperature experiment

CONCLUSION

This paper presented the results of a study investigating the influence of scale on the transient response of a sUAS rotor-motor system. The following are conclusions based upon this first analysis of the results:

- The coast-down process is more sensitive to rotor-motor size than the ramp-up process.
- The influence of all input factors should be further studied to determine the primary input variables to the transient response. The range of input values should be as wide as possible.
- Temperature and thermal management are important considerations for variable-speed motors, especially if they are growing and have no cooling other than the rotor windstream.

ACKNOWLEDGMENTS

This research was conducted under U.S. Army Research Office Grant No. W911NF-18-2-0025.

REFERENCES

[1] Federal Aviation Administration, "Small Unmanned Aircraft Systems." [Online]. Available: https://www.ecfr.gov/cgi-bin/text-idx?SID=0cb4bf8c80615851b712c2f4a9a289a9&mc=true&node=pt14.2.107&rgn=div5#sp14.2.107.a. [Accessed: 28-Jun-2017].

[2] K. Lang, "Amazon's Plea to Feds: Let Drones Deliver," *The Hill*, Apr-2015.

[3] "Amazon Prime Air," 2017. [Online]. Available: https://www.amazon.com/Amazon-Prime-Air/b?node=8037720011. [Accessed: 28-Jun-2017].

[4] Department of Defense, "Unmanned Systems Integrated Roadmap: 2013-2038," 2013.

[5] D. Gettinger, "Drone Spending in the Fiscal Year 2017 Defense Budget," Bard College, February 2016, 2016.

[6] N. Carey, "UPS-backed Rwandan blood deliveries show drones' promise, hurdles," *Reuters*, May-2016.

[7] M. Cutler, N. K. Ure, B. Michini, and J. P. How, "Comparison of Fixed and Variable Pitch Actuators for Agile Quadrotors," in *AIAA Guidance, Navigation, and Control Conference*, 2011, pp. 1–17.

[8] D. R. Weatherington, *Post Iraq and Afghanistan: Current and Future Roles for UAS and the Fiscal Year 2014 Budget Request*. 2013.

[9] J. Holden and N. Goel, "Fast-Forwarding to a Future of On-Demand Urban Air Transportation." Uber Elevate, Oct-2016.

[10] S. Bouabdallah and R. Siegwart, "Towards Intelligent Miniature Flying Robots.," in *Field and Service Robotics: Results of the 5th International Conference*, Port Douglas, Australia, 2005, pp. 429–440.

[11] K. Alexis, G. Nikolakopoulos, and A. Tzes, "Switching model predictive attitude control for a quadrotor helicopter subject to atmospheric disturbances," *Control Eng. Pract.*, vol. 19, no. 10, pp. 1195–1207, 2011.

[12] M. A. Mohd Basri, A. R. Husain, and K. A. Danapalasingam, "Enhanced Backstepping Controller Design with Application to Autonomous Quadrotor Unmanned Aerial Vehicle," *J. Intell. Robot. Syst. Theory Appl.*, 2014.

[13] R. Czyba, "Design of attitude control system for an UAV type-quadrotor based on dynamic contraction method," in *Advanced Intelligent Mechatronics, 2009. AIM 2009. IEEE/ASME International Conference on*, 2009, pp. 644–649.

[14] C. Nicol, C. J. B. Macnab, and A. Ramirez-Serrano, "Robust neural network control of a quadrotor helicopter," in *Electrical and Computer Engineering, 2008. CCECE 2008. Canadian Conference on*, 2008, pp. 1233–1238.

[15] M. Ouassaid, M. Cherkaoui, and Y. Zidani, "A nonlinear speed control for a PM synchronous motor using an adaptive backstepping control approach," in *Industrial Technology, 2004. IEEE ICIT'04. 2004 IEEE International Conference on*, 2004, vol. 3, pp. 1287–1292.

[16] W. Wang, X. Yuan, and J. Zhu, "Automatic PID tuning via differential evolution for quadrotor UAVs trajectory tracking," in *Computational Intelligence (SSCI), 2016 IEEE Symposium Series on*, 2016, pp. 1–8.

[17] S. Driessens and P. Pounds, "The triangular quadrotor: a more efficient quadrotor configuration," *IEEE Trans. Robot.*, vol. 31, no. 6, pp. 1517–1526, 2015.

[18] S. Driessens and P. E. I. Pounds, "Towards a more efficient quadrotor configuration," in *Intelligent Robots and Systems (IROS), 2013 IEEE/RSJ International Conference on*, 2013, pp. 1386–1392.

[19] P. Pounds and R. Mahony, "Design principles of large quadrotors for practical applications," in *2009 IEEE International Conference on Robotics and Automation*, 2009, pp. 3265–3270.

[20] P. Famouri, "Control of a Linear Permanent Magnet Brushless Dc Motor Via Exact Linearization Methods," *IEEE Trans. Encrgy Convers.*, vol. 7, no. 3, 1992.

[21] S. A. Kader, A. El-henawy, and A. N. Oda, "Quadcopter System Modeling and Autopilot Synthesis," *Int. J. Res. Technol.*, vol. 3, no. 11, pp. 9–14, 2014.

[22] A. Tayebi and S. Mcgilvray, "Attitude stabilization of a four-rotor aerial robot."

[23] P. Wang, Z. Man, Z. Cao, J. Zheng, and Y. Zhao, "Dynamics modelling and linear control of quadcopter," in *Advanced Mechatronic Systems (ICAMechS), 2016 International Conference on*, 2016, pp. 498–503.

[24] R. B. Sepe and J. H. Lang, "Real-Time Observer-Based (Adaptive) Control of a Permanent-Magnet Synchronous Motor without Mechanical Sensors," *IEEE Trans. Ind. Appl.*, 1992.

[25] V. Petrović, R. Ortega, and A. M. Stanković, "Interconnection and damping assignment approach to control of PM synchronous motors," *IEEE Trans. Control Syst. Technol.*, 2001.

[26] L. Heng, L. Meier, P. Tanskanen, F. Fraundorfer, and M. Pollefeys, "Autonomous Obstacle Avoidance and Maneuvering on a Vision-Guided MAV Using On-Board Processing," in *2011 IEEE International Conference on Robotics and Automation*, 2011, pp. 2472–2477.

[27] M. Dai, A. Keyhani, and T. Sebastian, "Fault Analysis of a PM Brushless DC Motor Using Finite Element Method," *IEEE Trans. ENERGY Convers.*, vol. 20, no. 1, 2005.

[28] A. S. Sekhar and B. S. Prabhu, "Condition monitoring of cracked rotors through transient response," *Mech. Mach. Theory*, vol. 33, no. 8, pp. 1167–1175, 1998.

[29] T. L. Davis, "Development and Characterization of a UAS Propulsion Test Bench," Master of Technology, Kent State University, 2018.

APPENDIX: ROTOR-MOTOR CONFIGURATION PROPERTIES

Rotor Properties

(1) TM-Rotor
15 x 5R, 2-blade

mass (m)	27.76	g
	1.9021E-03	slug
weight (W)	6.1248E-02	lbf
diameter (d)	15.0	in
	1.25	ft
area	1.227	ft^2
inertia (I)	2.171E-04	$slug.ft^2$

(2) TM-Rotor
15 x 5L, 2-blade

mass (m)	28.07	g
	1.9234E-03	slug
weight (W)	6.1932E-02	lbf
diameter (d)	15.0	in
	1.25	ft
area	1.227	ft^2
inertia (I)	2.243E-04	$slug.ft^2$

(3) Falcon Rotor
27 x 8.8R, 2-blade

mass (m)	97.98	g
	6.7136E-03	slug
weight (W)	2.1618E-01	lbf
diameter (d)	27.0	in
	2.25	ft
area	3.976	ft^2
inertia (I)	0.0025	$slug.ft^2$

(4) KDE Rotor
30.5 x 9.7L, 3-blade

mass (m)	222.53	g
	1.5248E-02	slug
weight (W)	4.9098E-01	lbf
diameter (d)	30.5	in
	2.54	ft
area	5.074	ft^2
inertia (I)	0.0064	$slug.ft^2$

Motor Properties

KDE "Mini" 4215XF-465

mass (m)	218.45	g
	0.0150	slug
weight (W)	0.4820	lbf
diameter (d)	48.3	mm
	0.1583	ft
inertia (I)	0.000047	$slug.ft^2$

T-Motor U7 KV280

mass (m)	255	g
	0.0175	slug
weight (W)	0.5626	lbf
diameter (d)	60.7	mm
	0.1992	ft
inertia (I)	0.000087	$slug.ft^2$

KDE 7215XF-135

mass (m)	555	g
	0.0380	slug
weight (W)	1.2245	lbf
diameter (d)	80.8	mm
	0.2651	ft
inertia (I)	0.000334	$slug.ft^2$

T-Motor P80 KV100

mass (m)	565	g
	0.0387	slug
weight (W)	1.2466	lbf
diameter (d)	91.6	mm
	0.3005	ft
inertia (I)	0.000437	$slug.ft^2$

KDE "Mega" 10218XF-105

mass (m)	1075	g
	0.0737	slug
weight (W)	2.3718	lbf
diameter (d)	109.1	mm
	0.3580	ft
inertia (I)	0.001180	$slug.ft^2$

Turnigy Rotomax 150cc

mass (m)	2530	g
	0.1734	slug
weight (W)	5.5821	lbf
diameter (d)	109.0	mm
	0.3576	ft
inertia (I)	0.002771	$slug.ft^2$